Earth and Planetary Science Letters 586 (2022) 117532

Contents lists available at ScienceDirect

Earth and Planetary Science Letters

www.elsevier.com/locate/epsl

Modelling evidence for late Eocene Antarctic glaciations

Jonas Van Breedam [a,*], Philippe Huybrechts [a], Michel Crucifix [b]

[a] Earth System Science and Departement Geografie, Vrije Universiteit Brussel, Brussels, Belgium
[b] Earth and Life Institute, Université catholique de Louvain, Louvain-la-Neuve, Belgium

ARTICLE INFO

Article history:
Received 16 October 2021
Received in revised form 10 March 2022
Accepted 3 April 2022
Available online 15 April 2022
Editor: Y. Asmerom

Keywords:
Antarctica
late Eocene
ice sheets
Eocene-Oligocene transition
emulator

ABSTRACT

It is generally believed that a large scale Antarctic ice sheet formed at the Eocene-Oligocene transition (34.44-33.65 Ma). However, oxygen isotope excursions during the late Eocene (38-34 Ma) and geomorphic evidence of glacial erosion suggest that there were ephemeral continental scale glaciations before the Oi-1 event. Here, we investigate the Antarctic ice sheet evolution over a multi-million year timescale during the late Eocene up to the early Oligocene with the most recent estimates of carbon dioxide evolution over this time period and different bedrock elevation reconstructions. A novel ice sheet-climate modelling approach is applied where the Antarctic ice sheet model VUB-AISMPALEO is coupled to the emulated climate from HadSM3 using the coupler CLISEMv1.0. Our modelling results show that short-lived continental scale Antarctic glaciation might have occurred during the late Eocene when austral summer insolation reached a minimum in a narrow range of carbon dioxide concentrations. The Antarctic ice sheet first reached the coast in Prydz Bay and later in the Weddell Sea region, supporting the glaciomarine sediments dated prior to the EOT.

1. Introduction

The Early Eocene Climatic Optimum (52-50 Ma) was the warmest long-term episode in Cenozoic climate history and was followed by a long-term cooling trend - interrupted by the Middle Eocene Climatic Optimum (~40 Ma) - culminating at the Eocene-Oligocene Transition (~34 Ma), when it is widely recognized that a continental scale Antarctic ice sheet was formed (Coxall et al., 2005; Lear et al., 2008). There is a long-standing discussion on the decisive actors favouring Antarctic ice sheet growth at the Eocene-Oligocene transition. The cooling and glaciation of the Antarctic continent has been attributed to a long-term declining trend in carbon dioxide concentrations as indicated by proxies (Pagani et al., 2011; Zhang et al., 2013; Tremblin et al., 2016) and supported by modelling studies (DeConto and Pollard, 2003a; Ladant et al., 2014). Others suggested that the cooling associated with the opening of the Antarctic Seaways and the thermal isolation of the Antarctic continent were the main driver for Antarctic glaciation (Kennett, 1977; Bijl et al., 2013). More recently, Goldner et al. (2014) concluded that oceanic cooling was a significant feedback on Antarctic ice sheet growth.

New insights suggest that the Southern Ocean cooling might have been caused by increased polar amplification with amplified temperature gradients and increased wind strengths that invigorated the Antarctic Circumpolar Current (Houben et al., 2019). Hence, the main driver of Antarctic glaciation would be atmospheric cooling rather than deepening of the Tasman gateway. On the other hand, the opening of the Southern Ocean gateways led to biological productivity changes and this might have caused a decrease in CO_2 concentrations (Scher and Martin, 2006), pointing towards an indirect causal effect of the ocean gateway opening. The CO_2 threshold for Antarctic ice sheet glaciation at the EOT is thought to have been somewhere between 790 ppmv (DeConto and Pollard, 2003a) and 900 ppmv (Ladant et al., 2014), and estimates of this threshold depend on the model and on the applied boundary conditions (Gasson et al., 2014).

Deep sea benthic foraminifera suggest a global cooling in combination with ice sheet growth at the Eocene-Oligocene Transition (EOT; ~34 Ma). The benthic oxygen isotope record is marked by a two-step increase of 1.5‰ in the benthic oxygen isotope record at 33.65 Ma. This marks the Oi-1 event, which is commonly interpreted as the signature of Antarctic ice sheet reaching a continental scale for the first time (Coxall et al., 2005; Lear et al., 2008). The transition of the Eocene hothouse to the Oligocene icehouse is preceded by the so called middle to late Eocene 'doubthouse' (Abels et al., 2011), when the climate cooled and ephemeral glaciations on Antarctica took place. The overall atmospheric CO_2 concentration trend was downwards, but strong oscillations occurred and CO_2 levels might have reached the glaciation threshold (Pagani et al., 2011).

* Corresponding author.
E-mail address: jonas.van.breedam@vub.be (J. Van Breedam).

https://doi.org/10.1016/j.epsl.2022.117532

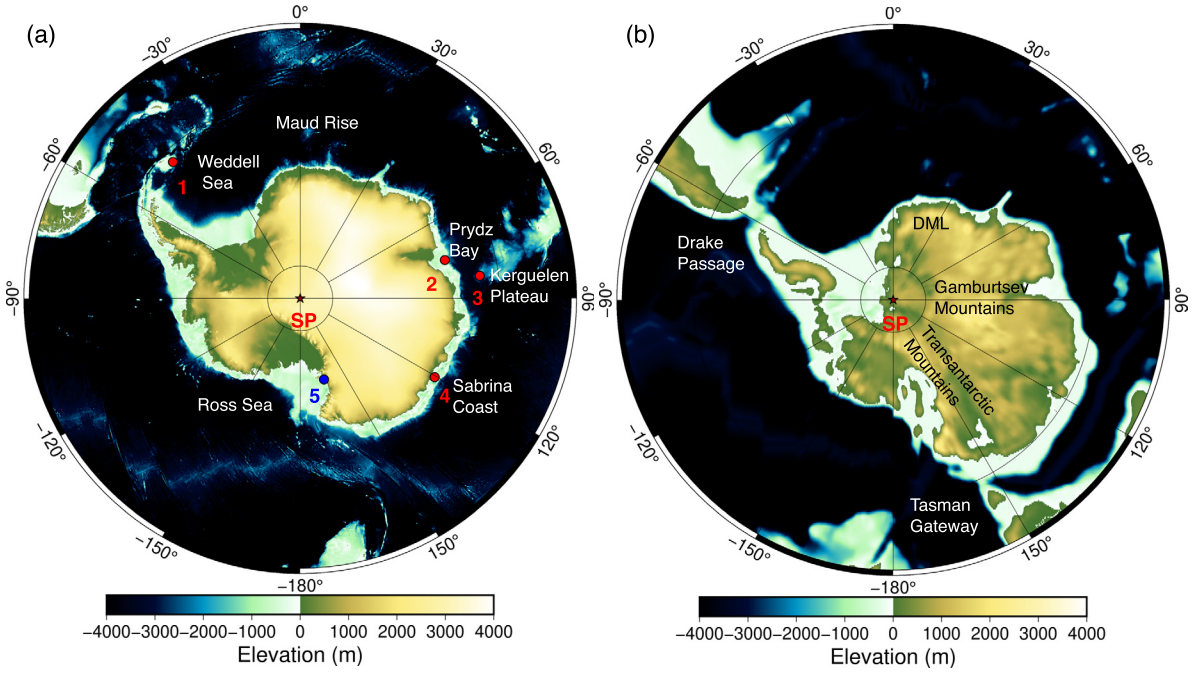

Fig. 1. (a): Polar stereographic projection south of 50°S for the present-day topography and bathymetry of the Southern Ocean and Antarctica. The red dots are locations where evidence for late Eocene glaciations is found: (1) sedimentological record from the Weddell Sea region (Carter et al., 2017), (2) sedimentological record from Prydz Bay (Passchier et al., 2017), (3) geochemical evidence from Kerguelen Plateau (Scher et al., 2014), (4) sedimentological record from Sabrina Coast (Gulick et al., 2017). The blue dot (5) indicates the location where the first glacial sediments date to 34.1 Ma (Galeotti et al., 2016). (b): Reconstructed palaeotopography and palaeobathymetry during the late Eocene. Bedrock reconstruction after Paxman et al. (2019) and palaeogeographic reconstruction after Baatsen et al. (2016). SP = South Pole, DML = Dronning Maud Land. (For interpretation of the colours in the figure(s), the reader is referred to the web version of this article.)

The first stages of mountain glaciation likely began on the Antarctic Peninsula between 37 Ma and 34 Ma (Anderson et al., 2011). These short-lived glaciations are thought to have been small and limited to the highest elevations of Antarctica. Recent interpretations of Cenozoic sedimentary records from the Southern Ocean (Gulick et al., 2017) and oxygen isotope records located close to the Antarctic continent (Scher et al., 2014) show evidence for ephemeral middle-late Eocene ice in Antarctica (Fig. 1). These late Eocene glaciations are consistent with estimates of global sea-level changes of up to 40 m (Peters et al., 2010). The Priabonian Oxygen Isotope Maximum (PrOM) event at 37.3 Ma is interpreted as a first continental scale glaciation (Scher et al., 2014). Carter et al. (2017) attributes the deposition of glacial eroded material in the Weddell Sea region between 36.5 Ma and 33 Ma to the existence of continental scale Antarctic glaciation well before the oxygen isotope excursion at the EOT. In the vicinity of Prydz Bay, glaciomarine sedimentation suggests that mountain glaciation was present at 35.9 Ma (Passchier et al., 2017) while in the Ross Sea, the first glacial sediments are only found around 34.1 Ma (Galeotti et al., 2016).

The geomorphic and isotopic evidence for late Eocene glaciations has not been supported by experiments with numerical models. Simulations suggest a sharp transition towards a glaciated state, and a strong hysteresis effect once the ice sheet reaches a continental scale (DeConto and Pollard, 2003b; Pollard and DeConto, 2005). This implies that once the ice sheet grows to a fully glaciated state, it is hard to make it disappear again. In this study, the potential for ephemeral late Eocene glaciations is investigated in order to see if the sedimentological data, that suggest continental scale ice sheet growth prior to the EOT, can be supported by a modelling effort. The dynamics of the Antarctic ice sheet will be assessed and insights in the timing and size of the ephemeral glaciations will be acquired. Therefore, we present transient ice sheet-climate simulations using a Gaussian process emulator over a multi-million year timescale starting during the late Eocene (38 Ma) up to the early Oligocene (32 Ma). We make use of recent CO_2 compilations in combination with the newest Antarctic bedrock topography reconstructions for the late Eocene.

2. Model description

The different models used in this study are the climate model HadSM3 and the ice sheet model AISMPALEO. The models interact with one another through the Gaussian process emulator CLISEMv1.0 (Van Breedam et al., 2021b).

2.1. Climate model HadSM3

The general circulation model HadSM3 (Williams et al., 2001) is used in this study to provide the climate forcing. The atmospheric component of the climate model has a horizontal resolution of 2.5° x 3.75°, with 19 levels in the vertical on a hybrid vertical coordinate (Pope et al., 2000). The slab ocean model lacks ocean dynamics and sea surface temperatures (SSTs) are prescribed based on a best fit from observations for the late Eocene between 36 Ma and 34 Ma (Evans et al., 2018; Fig. 2b). These SST are needed to calibrate the anomalous heat convergence in a coupled slab ocean-atmospheric model. The MOSES-1 land surface scheme is used to calculate the fluxes between the surface and the atmosphere (Cox et al., 1999). The albedo on the Antarctic continent is representative for tundra-like vegetation except where ice is present and the solar constant is 1360 $W\,m^{-2}$.

The palaeogeographic reconstruction for the simulations is based on the method presented in Baatsen et al. (2016) and makes use of the Gplates software. The reconstruction is representative for the continental configuration at 39 Ma. The reconstructed elevations take into account a middle to late Eocene mean sea level that was 100 m higher than today, combining the effects of no land ice, thermosteric sea-level rise from a warmer ocean and ocean basin size changes (Wright et al., 2020). The method gives the

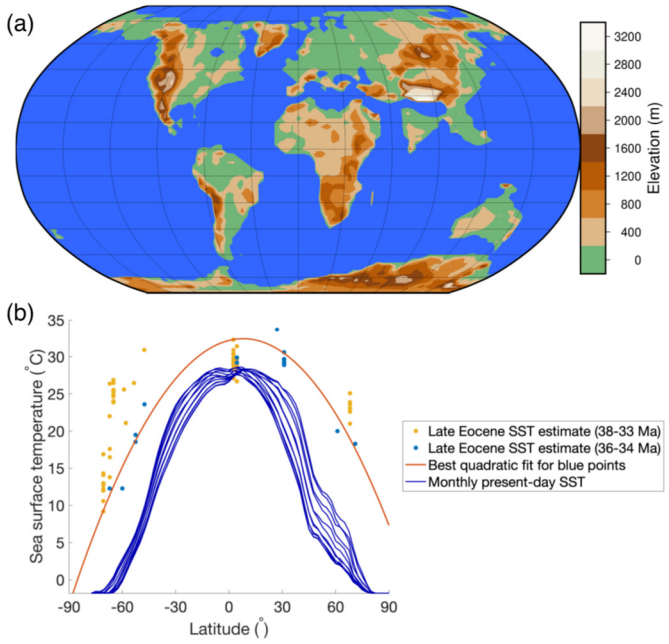

Fig. 2. (a) Palaeogeography and palaeotopography for the late Eocene using the van Hinsbergen et al. (2015) rotation. Reconstructions are performed with the GPlates software. The palaeotopography is derived from Baatsen et al. (2016). (b) Sea surface temperatures used as input for the slab ocean model as a best estimate (quadratic fit) from the compilation of Evans et al. (2018) for the period from 34 Ma to 36 Ma.

choice for different rotational models. We applied the one by van Hinsbergen et al. (2015). As a result of the rotational model, the position of the Antarctic continent is slightly shifted with respect to the present-day. The Antarctic bedrock elevation comes from the Wilson et al. (2012) maximum bedrock elevation reconstruction at 34 Ma. Additional sensitivity runs with the ice sheet model are performed for the Wilson et al. (2012) minimum bedrock topography reconstruction and the minimum and maximum bedrock elevation estimates from Paxman et al. (2019; Fig. 3). These reconstructions are based on erosion models and models that take into account thermal subsidence and plate movements. In order to capture the full uncertainty associated with the Wilson et al. (2012) and the Paxman et al. (2019) reconstructions, the high resolution reconstructions are regridded to the 40 km ice sheet model resolution. In each grid cell of the ice sheet model, the highest and lowest value for respectively the maximum and minimum bedrock topography estimates are selected and assigned to the ice sheet model grid. Overall the Paxman et al. (2019) bedrock topography reconstructions at 34 Ma have a lower topography than the Wilson et al. (2012) reconstruction. This is most obvious in West Antarctica and the Wilkes basin. The differences between the minimum and maximum bedrock topography estimate from Wilson et al. (2012) are most pronounced in West-Antarctica with variations exceeding 1000 m. Another remarkable difference is that the Paxman minimum bedrock topography lacks the Transantarctic Mountains, while the other five reconstructions show a significant elevation there.

2.2. Ice sheet model AISMPALEO

The Antarctic ice sheet model AISMPALEO is a three-dimensional thermomechanical ice sheet/ice shelf model (Huybrechts, 2002). The model has been used most recently for simulating ice sheet dynamics for periods in the past (Goelzer et al., 2016; Van Breedam et al., 2021a) and the future (Van Breedam et al., 2020). The Shallow Ice Approximation is used to calculate the grounded ice flow, resulting from internal deformation and basal sliding where the pressure melting point is reached. AISMPALEO includes an isostasy model taking into account the solid Earth response due to ice mass addition and removal. This component consists of a lithosphere with a certain rigidity on top of a viscous asthenosphere to allow for deviations from local isostatic loading. The surface mass balance is computed using the computationally efficient Positive Degree Day (PDD) method (Janssens and Huybrechts, 2000). This method calculates the yearly sum of daily average temperatures above 0 °C, which is used to determine the melt potential. To take into account the effect of random weather fluctuations and the daily cycle, the standard deviation of the mean daily temperature is included with a value of 4.2 °C. The difference in snow and ice albedo in the ice sheet model is taken into account by using a PDD factor for snow melting of 2.7 mm ice equivalent (i.e.) per °C per day and a PDD factor for ice melting of 7.9 mm i.e. per °C per day. Monthly mean temperature and precipitation are used from HadSM3 to estimate the PDD sum. The rain limit is chosen at 1 °C and determines whether precipitation falls as snow or as rain. A parameterization of meltwater retention allows runoff to be retarded and/or to eventually refreeze in the snowpack. The ice shelf model is included whenever the grounded ice reaches the ocean. The ocean was warm compared to the present-day. Since it is impossible to reconstruct these past shelf melt rates, a constant shelf melt rate of 10 m per year is applied everywhere. The grounding line is calculated in a one grid cell wide transition zone between the grounded ice and the floating ice where all stress components are considered. The ice shelves also lose mass by surface ablation. The ice sheet model is run at a resolution of 40 km to allow for long time integrations.

2.3. The Gaussian process emulator: CLISEMv1.0

We use the Gaussian process emulator CLISEMv1.0 to estimate the climate from a predefined number of climate model runs. The set-up of the emulator is identical to EMULATOR_20 calibrated on ice volume, presented in Van Breedam et al. (2021a, 2021b). In short, 100 experiments are performed with the climate model HadSM3 with each a different combination of orbital parameters, CO_2, and 20 predefined ice sheet geometries that differ in ice volume, albedo, elevation and vegetation (tundra albedo where no ice is present) on the Antarctic continent. The ice volume used in the emulator is between 0.236×10^6 km^3 and 32.9×10^6 km^3 for the smallest and largest ice sheet geometry, respectively. The ice sheet snapshots are chosen to have a good spread between all geometries in terms of ice volume. The CO_2 interval ranges from 550 ppmv to 1150 ppmv, roughly equivalent to 2 x pre-industrial CO_2 (280 ppmv) to 4 x pre-industrial CO_2. CLISEMv1.0 is calibrated based on the orbital parameters, the CO_2 concentration and the ice sheet volume of a training set of 100 experiments. After the calibration process, the emulator is able to predict the climatic model variables used by the ice sheet model (temperature and precipitation) for any combination of the external forcing parameters within the domain of the training set. All simulations are ran with a coupling time step of 500 years, since it has been shown that a larger timestep might overestimate the ice sheet response to the forcing (Van Breedam et al., 2021a).

3. Experimental set-up

The simulations span the interval between 38 Ma and 32 Ma, such as to include the cooling trend after the Mid Eocene Climatic Optimum (MECO; 40 Myr) and the EOT (defined between 34.44 Ma and 33.65 Ma in line with Hutchinson et al., 2021). The time interval also spans the entire Priabonian stage during which episodes of continental scale glaciations are observed in the geological record. The main external forcing for the multi-millennial

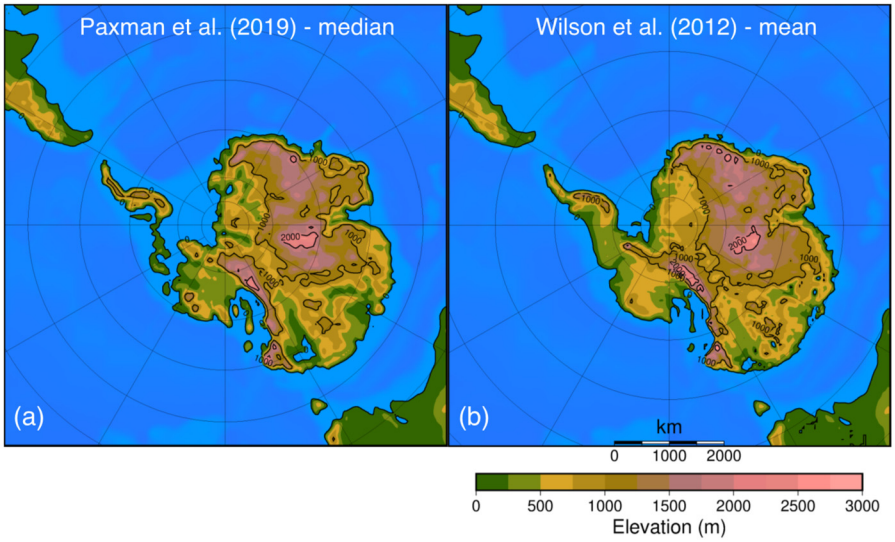

Fig. 3. Reconstructed bedrock topography and palaeogeography using the (a) Paxman et al. (2019) median bedrock topography and (b) the Wilson et al. (2012) mean bedrock topography. Note the Antarctic continental drift and the narrow Drake Passage and Tasman Gateway.

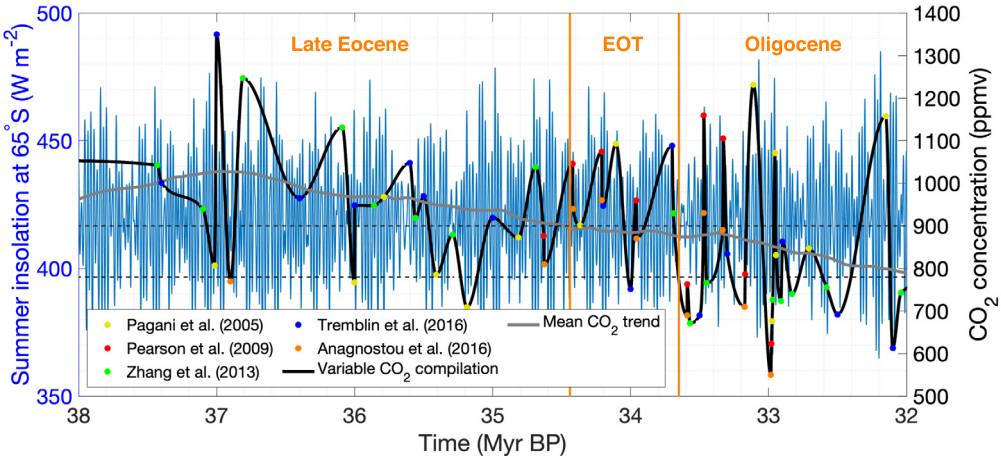

Fig. 4. CO_2 compilation based on data from Pagani et al. (2005), Pearson et al. (2009), Zhang et al. (2013), Anagnostou et al. (2016) and Tremblin et al. (2016). The solid black line shows the best fit for the CO_2 concentration through all data points. The median estimate from each study is chosen. The solid grey line shows the mean CO_2 concentration throughout the interval. Mean austral summer (December, January, February) insolation at 65°S is shown in blue. The dashed horizontal black lines indicate the presumed CO_2 glaciation threshold interval between 780 ppmv and 900 ppmv (DeConto and Pollard, 2003a; Ladant et al., 2014). The EOT interval is indicated by the orange vertical lines between 34.44 Ma and 33.65 Ma.

experiments comes from the orbital forcing and the greenhouse gases forcing (only carbon dioxide on these long timescales). At the MECO, it is thought that ice was not present on Antarctica and all ice sheet simulations start from ice-free conditions. The reconstructed CO_2 pathway is based on available data from Pagani et al. (2005), Pearson et al. (2009), Zhang et al. (2013), Anagnostou et al. (2016) and Tremblin et al. (2016). These data are reconstructed based on boron isotopes and carbon isotopes in alkenones and coccoliths. The mean CO_2 estimate is always taken from each of the studies. There are large uncertainties associated with the mean estimate (roughly between $\pm$200 ppmv to $\pm$500 ppmv), but since the errors differ for the different proxies and also as a function of time, it is chosen to perform all the simulations based on the mean CO_2 estimates. The resulting CO_2 forcing consists of a multi-proxy CO_2 reconstruction to investigate the temporal variations in CO_2, in combination with single proxy reconstruction from Zhang et al. (2013) and Tremblin et al. (2016). The orbital parameters are taken from Laskar et al. (2011), an improved orbital parameter solution compared to the study from Laskar et al. (2004). The error on the phases of the orbital solution is small up to 40 Ma ago. The main error arises from the uncertainty to tidal dissipation, a process that slows the Earth's rotation. For a tidal dissipation uncertainty up to 5%, the solutions for obliquity and precession remain valid up to 40 Myr. The mean austral summer insolation (December-January-February) at 65°S is calculated to indicate time periods when conditions were favourable for ice sheet growth. The absence of extreme insolation values caused by a low eccentricity around 33.65 Ma are thought to have aided ice sheet growth at the EOT (Coxall et al., 2005). (See Fig. 4.)

4. Results

The ice sheet evolution during the Priabonian and early Eocene from 38 Ma to 32 Ma is shown for the mean bedrock reconstruction from Wilson et al. (2012) and the median bedrock reconstruction from Paxman et al. (2019) in section 4.1. The uncertainty to different CO_2 reconstructions and to minimum and maximum estimates for the two bedrock topography reconstructions is investigated in section 4.2. Section 4.3 shows the influence of the

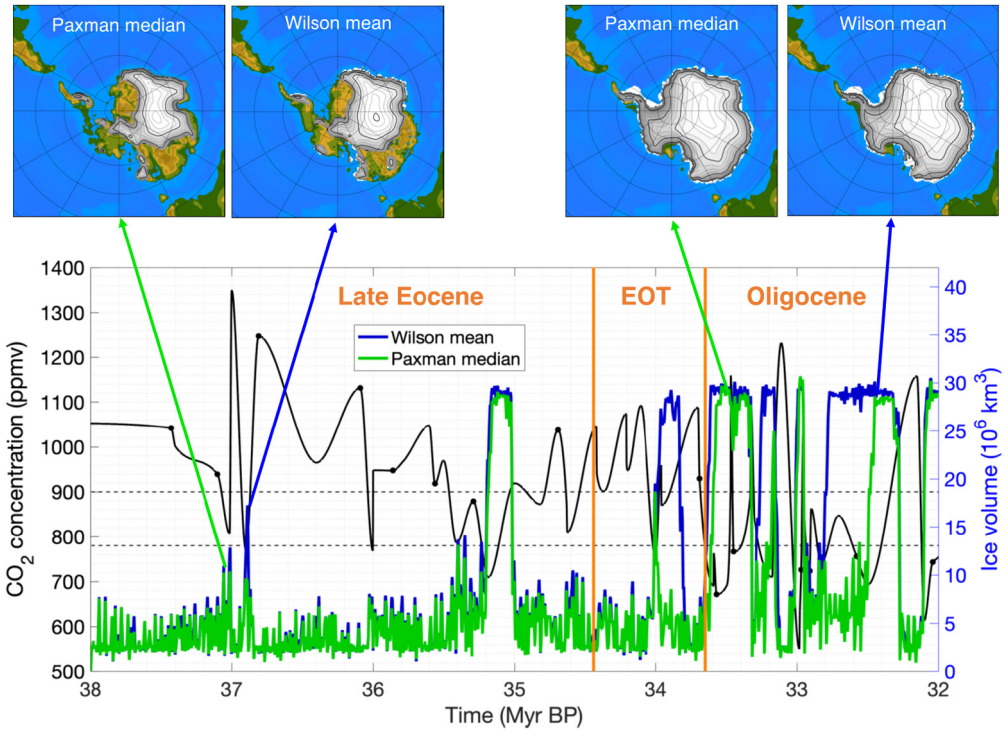

Fig. 5. CO_2 compilation based on data from Pagani et al. (2005), Pearson et al. (2009), Zhang et al. (2013), Anagnostou et al. (2016) and Tremblin et al. (2016). The size of the Antarctic ice sheet is shown at several snapshots for the Wilson mean and Paxman median bedrock topographies.

uncertainty in the dating of the carbon dioxide reconstructions during a short drop in the CO_2 reconstructions.

4.1. Ice sheet evolution using the CO_2 compilation for the mean bedrock topography reconstructions

The reconstructed CO_2 compilation is based on a best fit from the available CO_2 estimates from Pagani et al. (2005), Pearson et al. (2009), Zhang et al. (2013), Anagnostou et al. (2016) and Tremblin et al. (2016). All CO_2 data are the mean estimates based on different proxies. The simulated ice sheet evolution displays several partial glaciation episodes, which occur when CO_2 drops below identifiable thresholds (Fig. 5). The length of the CO_2 drop and the orbital forcing at this time determines the size of the ice sheet. For instance, the CO_2 minimum at 37.1 Ma is of similar magnitude as the CO_2 minimum at 36.0 Ma, but the cold austral summer configuration at 37.1 Ma allows for a stronger ice sheet growth. The ice sheet growth is most pronounced using the mean bedrock estimate from Wilson et al. (2012) and less widespread using the Paxman et al. (2019) median bedrock topography. The continental scale ice sheet is also melting again entirely when the CO_2 values exceed 900 to 1000 ppmv using respectively the Paxman et al. (2019) or Wilson et al. (2012) mean bedrock topography reconstructions, depending on the orbital forcing at the time. Continental-scale late Eocene glaciations are modelled during the period between 35.2 and 35 Ma and medium-sized ice sheet at 37.01 Ma and 36.90 Ma for both bedrock topographies.

Looking at the spatial pattern of glaciation, the ice sheet reaches the coast in the Weddell Sea region and Prydz Bay, but for a very limited part in the Ross Sea region. These icebergs transport ice rafted debris and therefore, the presence of iceberg calving is a good indicator for the localisation of glacial eroded sediments. The time evolution of the iceberg calving rate is visualised for two different sectors around the Antarctic ice sheet where evidence for pre-EOT glaciations is found. Our simulations show that the ice sheet first reaches the coast in Prydz Bay and only later in the other sectors such as the Weddell Sea and the Ross Sea when the ice sheet has a (nearly) continental size. Especially along Sabrina

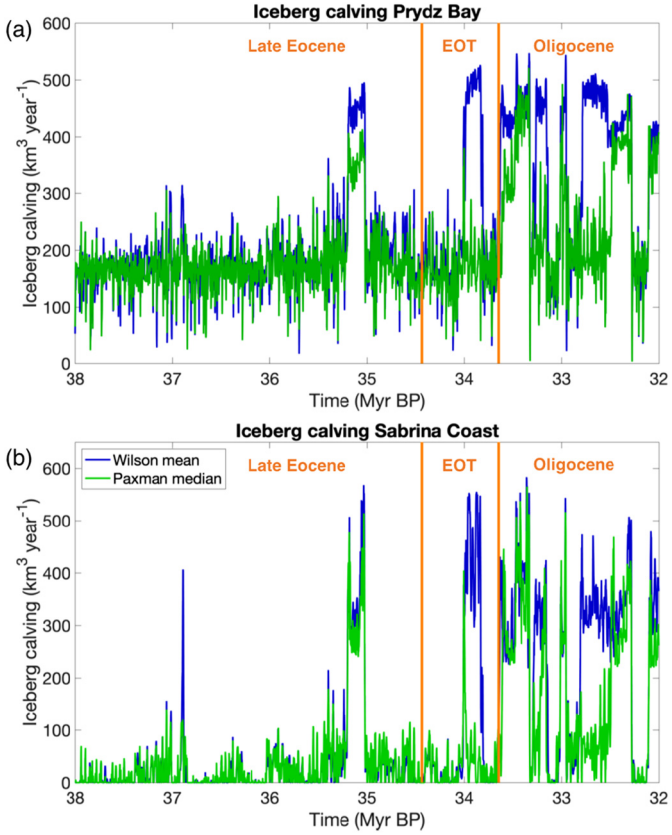

Fig. 6. Iceberg calving along (a) Prydz Bay and (b) Sabrina coast using the mean bedrock topography from Wilson et al. (2012) and the median bedrock topography from Paxman et al. (2019).

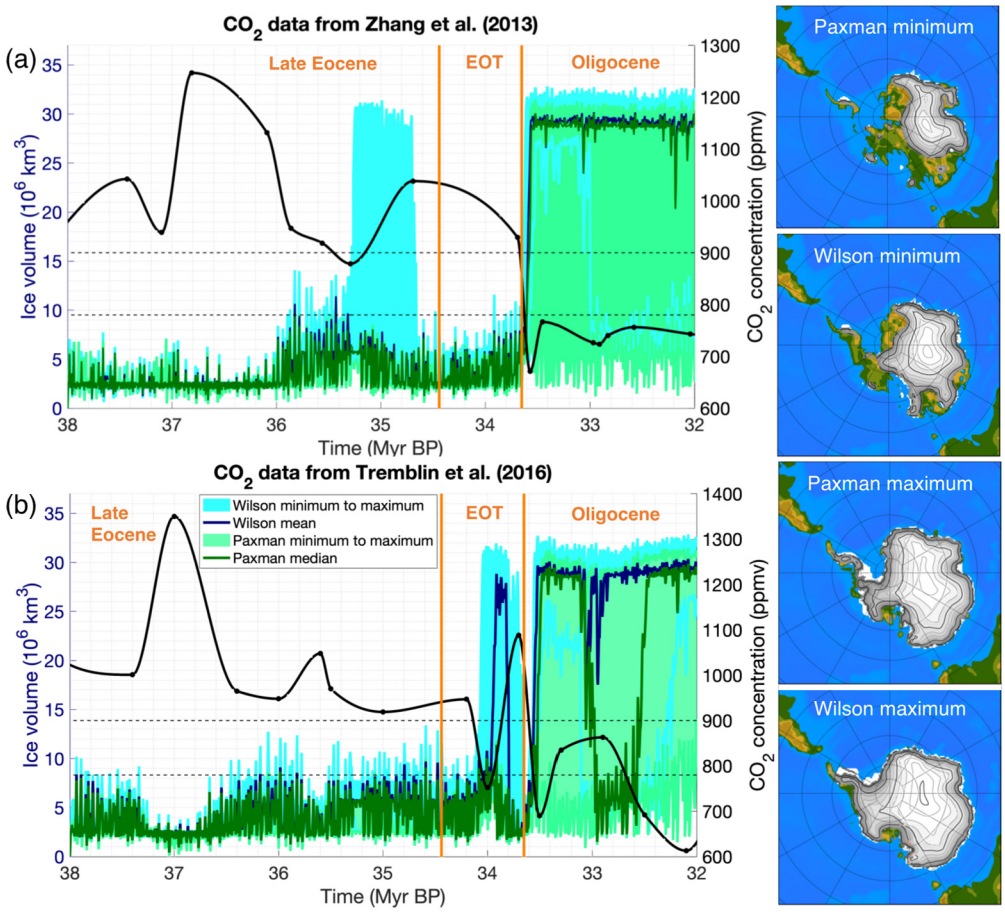

Fig. 7. Ice volume evolution for two different CO_2 curves and three different bedrock topography reconstructions. (a) CO_2 reconstruction based on data from Zhang et al. (2013). (b) CO_2 reconstruction based on data from Tremblin et al. (2016). The EOT glaciation threshold interval of 780 to 900 ppmv is shown by the dashed black lines. The light blue and light green colour shading represents the uncertainty in simulated ice volume between the minimum and maximum bedrock topography for respectively Wilson et al. (2012) and Paxman et al. (2019). The geometries on the right hand side represent the maximum size of the Antarctic ice sheet for the different input bedrock topographies.

Coast, icebergs calve each time the ice sheet volume increase to a medium sized ice sheet (Fig. 6). Passchier et al. (2017) suggested that the ice sheet grounding line reached the coast in Prydz Bay prior to the EOT based on a 400 m thick sedimentological record, while Gulick et al. (2017) identified several episodes with glacial eroded sediments during the late Eocene along Sabrina Coast. Our results confirm the existence of these glacial events reaching the coast prior to the EOT.

4.2. Sensitivity to different CO_2 curves and bedrock elevation reconstructions

The sensitivity to different CO_2 reconstructions is tested by running the simulations for the CO_2 reconstruction from Zhang et al. (2013) and Tremblin et al. (2016) that span the entire late Eocene period (38 – 34.44 Ma), the EOT (34.44 – 33.65 Ma) and the early Oligocene (33.65 Ma – 32 Ma). Additionally, the simulations are run for the minimum and maximum bedrock reconstructions from Wilson et al. (2012) and Paxman et al. (2019).

The resulting ice sheet evolution is visualised in Fig. 7 for the CO_2 data from Zhang et al. (2013) and Tremblin et al. (2016). The ice sheet does not grow to a fully glaciated state as long as CO_2 concentrations exceed 900 ppm. The threshold to continental scale glaciation is around 880 ppm for the Wilson maximum topography and the Paxman maximum topography reconstruction, while the CO_2 threshold for continental scale glaciation is below 750 ppm using the Wilson minimum topography. The CO_2 curve from Zhang et al. (2013) shows a first major decline in CO_2 around 33.6 Ma and the Antarctic ice sheet grows to a continental scale for all the different bedrock topographies, except the minimum estimate from Paxman et al. (2019). The CO_2 curve falls below the glaciation threshold of about 880 ppm at 35.35 Ma for the high bedrock topography estimates and the ice sheets grows towards a continental scale. The simulations forced by the CO_2 reconstruction from Tremblin et al. (2016) only cross the glaciation threshold around 34 Ma for the maximum and mean bedrock topography estimates from Wilson et al. (2012) and around 33.5 Ma for all but the minimum Paxman et al. (2019) bedrock topography estimate.

The uncertainty in the glaciation threshold between minimum and maximum bedrock topographies is quite large. The minimum bedrock topography from Paxman et al. (2019) does not allow for the build-up of a large ice sheet at the EOT because of the lack of the Transantarctic Mountains as a centre for the accumulation of ice. Using the maximum bedrock topographies, the continental scale ice sheet is more stable because of the larger glaciated area and the higher surface elevation of the ice sheet.

4.3. Sensitivity to the dating of the CO_2 reconstructions

In this section, the sensitivity of the ice sheet evolution to the dating of the carbon dioxide reconstructions is investigated. The short CO_2 drop around 36.9 Ma for the full CO_2 compilation is used to see if the timing of CO_2 highs and lows relative to the orbital forcing has a strong influence on the ice sheet growth. The

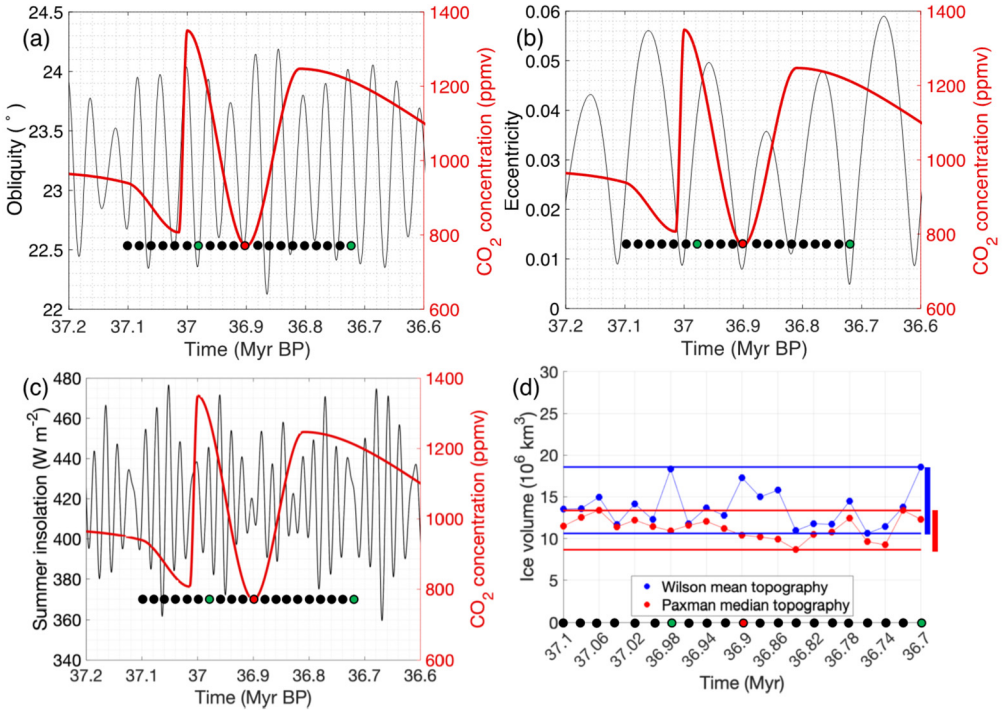

Fig. 8. Illustration of uncertainties in the dating of the CO_2 forcing relative to the orbital forcing and its influence on the ice sheet volume growth. The red dot indicates the present location of the minimum in the CO_2 concentration in the selected interval. The black dots indicate the location of the minimum for the shifted CO_2 curve with 20, 40, 60, 80, 100, 120, 140, 160, 180 and 200 kyr in both directions along the time axis. The green dots indicate the occurrence of a minimum in the CO_2 curve concomitant with a maximum ice sheet growth. (a) Shift in the CO_2 forcing compared to the obliquity. (b) Shift in the CO_2 forcing compared to the eccentricity. (c) Shift in the CO_2 forcing compared to the summer insolation at 65°S. (d) Maximum ice sheet volume for a shift in the CO_2 curves.

estimates of atmospheric CO_2 come with an uncertainty both in the exact value as in the timing. The uncertainty related to the timing is variable and is dependent on the age that is retrieved from the proxies. For CO_2 estimates during the late Eocene, the uncertainty in the timing of a CO_2 reconstructions goes up to 300 kyr (Anagnostou et al., 2016). The CO_2 curves are shifted along the time-axis with 20 kyr, 40 kyr, 60 kyr, 80 kyr, 100 kyr, 120 kyr, 140 kyr, 160 kyr, 180 kyr and 200 kyr in both directions. This way, the full uncertainty in the timing of the CO_2 curves is captured and the influence of the short-term (∼100 kyr) and long-term periods (∼405 kyr) of the eccentricity are explored, while the interval of 20 kyr captures the influence of the precession.

The ice sheet response is very sensitive to the timing of a CO_2 drop relative to the orbital forcing. Depending on the relative timing, the ice sheet volume ranges between 8.7 and 13.4×10^6 km^3 using the Paxman median topography and 10.6 and 18.6×10^6 km^3 using the Wilson mean topography. The CO_2 threshold falls to 770 ppmv (the glaciation threshold for the mean Wilson and Paxman topographies) at 36.9 Ma. However, only during very favourable orbital conditions (low values for the obliquity and the eccentricity and aphelion during austral summer), the ice sheet can build-up to a continental scale ice sheet.

It takes typically about 50 kyr to build-up a continental scale Antarctic ice sheet. That means that the optimal orbital parameters need to be sustained for a similar time in order that the ice-albedo feedback and the height-mass balance feedback are able to make the ice sheet grow beyond a critical threshold. Since the precession and the obliquity have a shorter period than the typical time to initiate the feedbacks involved in ice sheet growth, the role of the eccentricity is significant. The eccentricity determines the amplitude of the insolation curve. For a high eccentricity, the austral summer insolation is minimal in combination with low obliquity and the position of the Earth in aphelion in austral summer. However, the opposite is true about 10 kyr later when the position of the Earth is in perihelion during the austral summer, leading to a very high insolation in austral summer. Between 37.2 Ma and 36.6 Ma, the lowest relative maximum in the ∼405 kyr eccentricity cycle exceeds 0.035 and the ice sheet does not grow to a full continental scale, even for a low obliquity and the Earth in aphelion during the austral summer (Fig. 8). Because of the long response time of ice sheets to the forcing, the insolation curve needs to remain low (below levels that would cause substantial ice loss) for more than 10 kyr and hence a low eccentricity is necessary to induce glacial conditions. In this case, the ice sheet does not melt much in the absence of a summer insolation maximum and continues to grow during the next insolation minimum. Since the minimum summer insolation is not sustained for a sufficient time during the selected interval, the maximum ice sheet growth is achieved during minima in the obliquity and minima in the eccentricity and stays below the continental scale (Fig. 8).

Overall, by just changing the timing of the short drop in the CO_2 curve relative to the insolation forcing, the ice sheet geometry ranges from isolated ice caps in Dronning Maud Land and the Gamburtsev Mountains up to an ice sheet that covers about half of the continent for both the Wilson mean bedrock topography and the Paxman median bedrock topography.

5. Discussion

Although the overall trend in atmospheric CO_2 concentrations is declining throughout the late Eocene, there is a large temporal variability, especially when combining the atmospheric CO_2 estimates from different sources. Using these temporally variable CO_2 reconstructions, the Antarctic ice sheet grows to a (nearly) continental scale and declines when CO_2 values exceed a threshold. It appears that our estimates of the CO_2 threshold are highly sensitive to the applied bedrock topography. The threshold to full glaciation for the lowest bedrock topography is below 620 ppmv,

Table 1
The different thresholds in atmospheric CO_2 concentrations for a given bedrock topography leading to glaciation of the Antarctic continent. In case multiple thresholds are identified for different values of the orbital forcing, a range in the CO_2 threshold to glaciation is given.

Bedrock topography	CO_2 threshold to glaciation (ppmv)
Minimum (Paxman et al., 2019)	< 620
Minimum (Wilson et al., 2012)	680
Median (Paxman et al., 2019)	680-750
Mean (Wilson et al., 2012)	700-800
Maximum (Paxman et al., 2019)	700
Maximum (Wilson et al., 2012)	800-880

while the ice sheet can grow to a continental scale for an atmospheric CO_2 concentration of about 880 ppmv using the highest bedrock topography (Table 1). The experiments forced by the variable orbital parameters and CO_2 reconstructions indicate that there is a range in the CO_2 threshold to glaciation for a given bedrock topography depending on the orbital forcing. The ice sheet volume at the EOT is also dependent on the bedrock topography used and ranges from 14×10^6 km^3 for the Paxman et al. (2019) minimum topography up to 33×10^6 km^3 for the Wilson et al. (2012) maximum bedrock topography. According to Wilson et al. (2013), the simulated ice sheet volume at the EOT could have ranged between 33 and 36×10^6 km^3 in case the entire land area would have been ice covered. The simulated continental-scale ice sheet volume for the Paxman et al. (2019) median bedrock topography is 30×10^6 km^3. This is exactly between the simulated ice volume of 28×10^6 km^3 and 32×10^6 km^3 for the same topography (Paxman et al., 2020), where the lower volume estimate came from simulations forced with a CO_2 concentration of 840 ppmv and the higher volume estimate for a CO_2 forcing of 280 ppmv.

In our simulations, the uncertainty in the estimates of the CO_2 reconstructions itself is not investigated. Steinthorsdottir et al. (2016) found that terrestrial CO_2 proxies indicate significant lower CO_2 values during the late Eocene and Oligocene than marine-based CO_2 proxies. Recently, a reassessment of the uncertainty of the available CO_2 proxies based on carbon isotopes in alkenones and boron isotopes in planktic foraminifera was made (Rae et al., 2021). Although the reliability of their updated CO_2 reconstructions before the Miocene decreases, the new atmospheric CO_2 estimates are generally lower. This implies that the threshold to continental-scale glaciation might have been reached more frequently during the period prior to the EOT and for lower elevations of the bedrock topography.

We have used prescribed CO_2 variations to force the climate. Possibly, CO_2 variations could have occurred on an orbital timescale in a similar way as during the Quaternary (Lisiecki, 2010). Specifically, the CO_2 variations at around 37 Ma have a period of about 100 kyr or about an eccentricity cycle. It is proposed that eccentricity has paced the carbon cycle during the late Eocene to early Oligocene, with a strong influence of the continental ice volume, atmospheric circulation patterns and tectonic uplift on the interaction between the carbon cycle and the climate (De Vleeschouwer et al., 2020).

As shown during short-term drops in the CO_2 forcing, the role of the orbital parameters configuration is substantial. The austral summer insolation is paced by the precession, but the ice sheet can grow most when eccentricity is low. The coldest austral summers occur with a combination of high eccentricity, low obliquity and aphelion during the austral summer. In the simulations from DeConto and Pollard (2003b) the ice sheet responds quickly to this cold summer orbit and grows over most of East Antarctica. Their simulations were however based on snapshot experiments and not integrated over an eccentricity cycle. Liebrand et al. (2011) found that Antarctic ice sheet expansion during the Miocene was mostly governed by the long-term eccentricity period (400 kyr). Right before the eccentricity reached the minimum, the ice sheet rapidly expanded. The correlation between low eccentricity and maximum ice sheet advance was also supported by Levy et al. (2016) during the early to mid-Miocene.

The simulations in this study showed that several continental scale ice sheets have been modelled prior to the EOT using the median and mean bedrock topography estimates from Paxman et al. (2019) and Wilson et al. (2012). Using our independent full CO_2 reconstruction, continental scale glaciations are modelled around 37.01-36.9 Myr and 35.2-35.0 Myr ago. The benthic δ^{18}O excursion during the PrOM, indicating ice volume expansion and/or ocean cooling, occurred around 37.3 Ma and lasted about 140 kyr (Scher et al., 2014). The Vonhof cooling event ($\sim$35.8 Ma) is a 1-kyr long event observed as an increase of $\sim$0.5‰ in the δ^{18}O record and most likely explained by an increase in the volume of terrestrial ice (Vonhof et al., 2000; Śliwińska et al., 2019). The reason for the cooling event might have been a decrease in carbon dioxide concentrations or a prolonged period of high comet influx that caused the climate to cool (Vonhof et al., 2000). Given the uncertainty in the dating of both the benthic δ^{18}O record and the CO_2 reconstructions, our modelled glaciation events occur at a time close to the observed δ^{18}O excursions at the PrOM and the Vonhof cooling event. At 36 Ma, global sea-level is thought to have lowered by about 40 m, most likely due to ice sheet volume changes on Antarctica (Peters et al., 2010). Tibbett et al. (2021) identified warming intervals near Prydz Bay at 35.7 Ma and 34.7 Ma, before and after the glaciation that is present using the full CO_2 compilation.

Our simulations show that the ice sheet plausibly grew to a continental scale prior to the EOT for the mean and maximum bedrock topographies (but not for the minimum bedrock topographies) and declined again when CO_2 values exceeded the bedrock dependent CO_2 threshold. The ephemeral nature of the early Cenozoic Antarctic ice sheet is a remarkable finding, which may seem to contradict earlier findings that the Antarctic ice sheet was very stable once it grew to a continental scale (DeConto and Pollard, 2003b; Ladant et al., 2014). However, these studies did not investigate the sensitivity of the early Cenozoic ice sheet for temporally variable CO_2 reconstructions. Threshold behaviour was identified with a strong hysteresis between ice sheet growth and ice sheet decline (Pollard and DeConto, 2005). Gasson et al. (2016) modelled a similar behaviour for the Antarctic ice sheet during the Miocene with a strong variability in a narrow range of carbon dioxide concentrations.

Simulating the Antarctic ice sheet evolution on a multi-million year timescale requires some considerations about the erosion of the bedrock. Each time the ice sheet grows and declines, it partially erodes the underlying surface. As a consequence of the erosion, the land surface will also experience uplift due to mass unloading. Therefore, the assumption of a fixed bedrock topography is not entirely realistic. The maximum bedrock topography estimate is a reasonable estimate for initial conditions, but throughout time the bedrock erodes and the surface topography lowers. However, erosion of the land surface is a very slow process and the differences might be minor on a timescale of a few million years. The land area at the EOT was about 25% larger at the EOT than at the present-day, with an average decrease in the bed elevation of about 200 m over the last 34 Myr (Paxman et al., 2019). The higher topography also made the Antarctic ice sheet prone to grow for higher CO_2 concentrations than during later periods such as the Miocene when erosion had lowered the land.

Our modelling approach did not include a dynamic ocean model and therefore, the bulk ocean temperatures are not calculated throughout time and ocean circulation is not considered. This is arguably the largest caveat of this study because of the ocean's influence on the climate. Gasson et al. (2014) used HadCM3L with

a dynamic ocean to determine the atmospheric CO_2 threshold to glaciation and found it to be lower than 560 ppmv. In their study, the boundary conditions were different, most notably the orbital parameters, which were taken at their present-day values. The simulations were also one-way forced, meaning that the ice-albedo feedback was not taken into account. Therefore, the difference in model response cannot uniquely be attributed to the inclusion of a dynamic ocean model. Varying oceanic temperatures could also have influenced the ice shelf melt rate, even though this is of lesser importance in this study because the simulated Antarctic glaciation is largely terrestrial and driven by the surface mass balance. Another process connected to a dynamic ocean is the influence of freshwater fluxes originating from the ice sheet on Antarctic bottom water formation. It is thought that the release of freshwater fluxes influences the ocean circulation and cools the ocean (Goldner et al., 2014). However, these feedbacks play on a shorter, millennial timescale and only temporarily influence the climate (Van Breedam et al., 2020).

6. Conclusions

In this study, we have applied a new method to simulate ice-sheet climate interactions on a multi-million year timescale to the late Eocene to investigate the potential for ephemeral glaciations prior to the EOT. The geographical setting of the Antarctic continent is chosen to be representative of the late Eocene. Six different new bedrock elevation reconstructions are used to test the influence of the elevation on the ice sheet initiation. In combination with a set of recent CO_2 reconstructions, we tested the sensitivity of the early Cenozoic Antarctic ice sheet to the palaeoenvironment and investigated the potential to model late Eocene glaciations.

The existence of short-lived (nearly) continental scale glaciations are identified during time periods when the CO_2 level dropped below a threshold value of about 750-900 ppm, depending on the applied bedrock topography. It is found that the short-lived glaciations are most susceptible to grow during eccentricity minima. These glaciations occur in reasonable agreement to the timing of the PrOM oxygen isotope excursion around 37 Ma and the benthic $\delta^{18}O$ excursion around 35 Ma, known as the Vonhof cooling event. In between these glacial phases, CO_2 levels would have been higher and the continental scale ice sheet could melt when a CO_2 threshold was exceeded during a warm austral summer orbit.

Using the different CO_2 reconstructions and bedrock elevation estimates, a continental-scale glaciation is modelled for all simulations around the EOT when the CO_2 concentrations drop significantly, except for the Paxman minimum bedrock topography. The glaciation threshold is however strongly dependent on the bedrock topography used. For the minimum bedrock topographies, the CO_2 threshold is not reached during the late Eocene, but only at the EOT and for the Paxman minimum bedrock topography, CO_2 concentrations need to further decline below 650 ppmv to initiate a continental scale ice sheet.

CRediT authorship contribution statement

Jonas Van Breedam: Conceptualization, Investigation, Methodology, Software, Writing – original draft. **Philippe Huybrechts:** Methodology, Project administration, Supervision, Writing – review & editing. **Michel Crucifix:** Methodology, Software, Supervision, Writing – review & editing.

Data availability

The model code CLISEMv1.0 used to provide the climate forcing for the multi-million year simulations is available on https://doi.org/10.5281/zenodo.5245156. All model output data is available upon request.

Declaration of competing interest

The authors declare that they have no known competing financial interests or personal relationships that could have appeared to influence the work reported in this paper.

Acknowledgement

Jonas Van Breedam acknowledges support from project G091820N, funded by the Research Foundation Flanders (FWO Vlaanderen). Michel Crucifix is funded as Research Director with the Belgian National Fund of Scientific Research FNRS.

References

Abels, H.A., Dupont-Nivet, G., Xiao, G., Bosboom, R., 2011. Set-wise change of Asian interior climate preceding the Eocene-Oligocene Transition (EOT). Palaeogeogr. Palaeoclimatol. Palaeoecol. 299, 399–412. https://doi.org/10.1016/j.palaeo.2010.11.028.

Anagnostou, E., John, E.H., Edgar, K.M., Foster, G.L., Ridgwell, A., Inglis, G.N., Pancost, R.D., Lunt, D.J., Pearson, P.N., 2016. Changing atmospheric CO_2 concentration was the primary driver of early Cenozoic climate. Nature 533, 380–384. https://doi.org/10.1038/nature17423.

Anderson, J.B., Warny, S., Askin, R.A., Wellner, J.S., Bohaty, S.M., Kirshner, A.E., Livsey, D.N., Simms, A.R., Smith, T.R., Ehrmann, W., Lawver, L.A., Barbeau, D., Wise, S.W., Kulhanek, D.K., Weaver, F.M., Majewski, W., 2011. Progressive Cenozoic cooling and the demise of Antarctica's last refugium. Proc. Natl. Acad. Sci. USA 108, 11356–11360. https://doi.org/10.1073/pnas.1014885108.

Baatsen, M., van Hinsbergen, D.J.J., von der Heydt, A.S., Dijkstra, H.A., Sluijs, A., Abels, H.A., Bijl, P.K., 2016. Reconstructing geographical boundary conditions for palaeoclimate modelling during the Cenozoic. Clim. Past 12, 1635–1644. https://doi.org/10.5194/cp-12-1635-2016.

Bijl, P.K., Bendle, J.A.P., Bohaty, S.M., Pross, J., Schouten, S., Tauxe, L., Stickley, C.E., McKay, R.M., Röhl, U., Olney, M., Sluijs, A., Escutia, C., Brinkhuis, H., Expedition 318 Scientists, 2013. Eocene cooling linked to early flow across the Tasmanian Gateway. Proc. Natl. Acad. Sci. USA 110, 9645–9650. https://doi.org/10.1073/pnas.1220872110.

Carter, A., Roley, T.R., Hillenbrand, C.-D., Rittner, M., 2017. Widespread Antarctic glaciation during the late Eocene. Earth Planet. Sci. Lett. 458, 49–57. https://doi.org/10.1016/j.epsl.2016.10.045.

Cox, P.M., Betts, R.A., Bunton, C.B., Essery, R.L.H., Rowntree, P.R., Smith, J., 1999. The impact of new land surface physics on the GCM simulation of climate and climate sensitivity. Clim. Dyn. 15, 183–203. https://doi.org/10.1007/s003820050276. 590.

Coxall, H.K., Wilson, P.A., Pälike, H., Lear, C.H., Backman, J., 2005. Rapid stepwise onset of Antarctic glaciation and deeper calcite compensation depth in the Pacific Ocean. Nature 433, 53–57. https://doi.org/10.1038/nature03135.

DeConto, R.M., Pollard, D., 2003a. Rapid Cenozoic glaciation of Antarctica induced by declining atmospheric CO_2. Nature 421, 245–249. https://doi.org/10.1038/nature01290.

DeConto, R.M., Pollard, D., 2003b. A coupled climate-ice sheet modeling approach to the Early Cenozoic history of the Antarctic ice sheet. Palaeogeogr. Palaeoclimatol. Palaeoecol. 198, 39–52. https://doi.org/10.1016/S0031-0182(03)00393-6.

De Vleeschouwer, D., Drury, A.J., Vahlenkamp, M., Rochholz, F., Liebrand, D., Pälike, H., 2020. High-Latitude biomes and rock weathering mediate climate-carbon cycle feedbacks on eccentricity timescales. Nat. Commun. 11, 5013. https://doi.org/10.1038/s41467-020-18733-w.

Evans, D., Badger, M.P.S., Foster, G.L., Henehan, M.J., Lear, C.H., Zachos, J.C., 2018. No substantial long term bias in the Cenozoic foraminifera oxygen-isotope record. Nat. Commun. 9, 2875. https://doi.org/10.1038/s41467-018-05303-4.

Galeotti, S., DeConto, R., Naish, T., Stocchi, P., Florindo, F., Pagani, M., Barrett, P., Bohaty, S.M., Lanci, L., Pollard, D., Sandroni, S., Talarico, F.M., Zachos, J.C., 2016. Antarctic Ice Sheet variability across the Eocene-Oligocene boundary climate transition. Science 352, 76–80. https://doi.org/10.1126/science.aab0669.

Gasson, E., Lunt, D.J., DeConto, R., Goldner, A., Heinemann, M., Huber, M., LeGrande, A.N., Pollard, D., Sagoo, N., Siddall, M., Winguth, A., Valdes, P.J., 2014. Uncertainties in the modelled CO_2 threshold for Antarctic glaciation. Clim. Past 10 (2), 451–466. https://doi.org/10.5194/cp-10-451-2014.

Gasson, E., DeConto, R.M., Pollard, D., Levy, R.H., 2016. Dynamic Antarctic ice sheet during the early to mid-Miocene. Proc. Natl. Acad. Sci. USA 113, 3459–3464. https://doi.org/10.1073/pnas.1516130113.

Goelzer, H., Huybrechts, P., Loutre, M.-F., Fichefet, T., 2016. Last interglacial climate and sea-level evolution from a coupled ice sheet–climate model. Clim. Past 12, 2195–2213. https://doi.org/10.5194/cp-12-2195-2016.

Goldner, A., Herold, N., Huber, M., 2014. Antarctic glaciation caused ocean circulation changes at the Eocene-Oligocene transition. Nature 511, 574–577. https://doi.org/10.1038/nature13597.

Gulick, S.P.S., Shevenell, A.E., Montelli, A., Fernandez, R., Smith, C., Warny, S., Bohaty, S.M., Sjunneskog, C., Leventer, A., Frederick, B., Nlankenship, D.D., 2017. Initiation and long-term instability of the East Antarctic Ice Sheet. Nature 552, 225–229. https://doi.org/10.1038/nature25026.

Houben, A.J.P., Bijl, P.K., Sluijs, A., Schouten, S., Brinkhuis, H., 2019. Late Eocene Southern Ocean cooling and invigoration of circulation preconditioned Antarctica for full-scale glaciation. Geochem. Geophys. Geosyst. 20, 2214–2234. https://doi.org/10.1029/2019GC008182.

Hutchinson, D.K., Coxall, H.K., Lunt, D.J., Steinthorsdottir, M., de Boer, A.M., Baatsen, M., von der Heydt, A., Huber, M., Kennedy-Asser, A.T., Kunzmann, L., Ladant, J.-B., Lear, C.H., Moraweck, K., Pearson, P.N., Piga, E., Pound, M.J., Salzmann, U., Scher, H.D., Sijp, W.P., Śliwińska, K.K., Wilson, P.A., Zhang, Z., 2021. The Eocene–Oligocene transition: a review of marine and terrestrial proxy data, models and model–data comparisons. Clim. Past 17, 269–315. https://doi.org/10.5194/cp-17-269-2021.

Huybrechts, P., 2002. Sea-level changes at the LGM from ice-dynamic reconstructions of the Greenland and Antarctic ice sheets during the glacial cycles. Quat. Sci. Rev. 21 (1–3), 203–231. https://doi.org/10.1016/S0277-3791(01)00082-8.

Janssens, I., Huybrechts, P., 2000. The treatment of meltwater retention in mass-balance parameterizations of the Greenland ice sheet. Ann. Glaciol. 31, 133–140. https://doi.org/10.3189/172756400781819941.

Kennett, J.P., 1977. Cenozoic evolution of Antarctic glaciation, the circum-Antarctic Ocean, and their impact on global paleoceanography. J. Geophys. Res. 82, 3843–3860. https://doi.org/10.1029/JC082i027p03843.

Ladant, J-B., Donnadieu, Y., Lefebvre, V., Dumas, C., 2014. The respective role of atmospheric carbon dioxide and orbital parameters on ice sheet evolution at the Eocene-Oligocene transition. Paleoceanography 29, 810–823. https://doi.org/10.1002/2013PA002593.

Laskar, J., Robutel, P., Joutel, F., Gastineau, M., Correia, A.C.M., Levrard, B., 2004. A long-term numerical solution for the insolation quantities of the Earth. Astron. Astrophys. 428, 261–285. https://doi.org/10.1051/0004-6361:20041335.

Laskar, J., Fienga, A., Gastineau, M., Manche, H., 2011. La2010: a new orbital solution for the long-term motion of the Earth. Astron. Astrophys. 532, A89. https://doi.org/10.1051/0004-6361/201116836.

Lear, C.H., Bailey, T.R., Pearson, P.N., Coxall, H.K., Rosenthal, Y., 2008. Cooling and ice growth across the Eocene-Oligocene transition. Geology 36, 251–254. https://doi.org/10.1130/G24584A.1.

Levy, R., Harwood, D., Florindo, F., Sangiorgi, F., Tripati, R., von Eynatten, H., Gasson, E., Kuhn, G., Tripati, A., DeConto, R., Fielding, C., Field, B., Golledge, N., McKay, R., Naish, T., Olney, M., Pollard, D., Schouten, S., Talarico, F., Warny, W., Willmott, V., Acton, G., Panter, K., Paulsen, T., Taviani, M., SMS Science Team, 2016. Antarctic ice sheet sensitivity to atmospheric CO_2 variations in the early to mid-Miocene. Proc. Natl. Acad. Sci. USA 113, 3453–3458. https://doi.org/10.1073/pnas/1516030113.

Liebrand, D., Lourens, L.J., Hodell, D.A., de Boer, B., van de Wal, R.S.W., Pälike, H., 2011. Antarctic ice sheet and oceanographic response to eccentricity forcing during the early Miocene. Clim. Past 7, 869–880. https://doi.org/10.5194/cp-7-869-2011.

Lisiecki, L.E., 2010. A benthic δ^{13}C-based proxy for atmospheric pCO_2 over the last 1.5 Myr. Geophys. Res. Lett. 37, L21708. https://doi.org/10.1029/2010GL045109.

Pagani, M., Zachos, J.C., Freeman, K.H., Tipple, B., Bohaty, S., 2005. Marked decline in atmospheric dioxide concentrations during the Paleogene. Science 309, 600–603. https://doi.org/10.1126/science.1110063.

Pagani, M., Huber, M., Zhonghui, L., Bohaty, S.M., Henderiks, J., Sijp, W., Krishnan, S., DeConto, R.M., 2011. The role of carbon dioxide during the onset of Antarctic glaciation. Science 334, 1261–1264. https://doi.org/10.1126/science.1203909.

Passchier, S., Ciarletta, D.J., Miriagos, T.E., Bijl, P.K., Bohaty, S.M., 2017. An Antarctic stratigraphic record of stepwise ice growth through the Eocene-Oligocene transition. GSA Bull. 129, 318–330. https://doi.org/10.1130/B31482.1.

Paxman, G.J.G., Jamieson, S.S.R., Hochmuth, K., Gohl, K., Bentley, M.J., Leitchenkov, G., Ferraccioli, F., 2019. Reconstructions of Antarctic topography since the Eocene-Oligocene boundary. Palaeogeogr. Palaeoclimatol. Palaeoecol. 535, 109346. https://doi.org/10.1016/j.palaeo.2019.109346.

Paxman, G.J.G., Gasson, E.G.W., Jamieson, S.S.R., Bentley, M.J., Ferraccioli, F., 2020. Long-term increase in Antarctic ice sheet vulnerability driven by bed topography evolution. Geophys. Res. Lett. 47, e2020GL090003. https://doi.org/10.1029/2020GL090003.

Pearson, P.N., Foster, G.L., Wade, B.S., 2009. Atmospheric carbon dioxide through the Eocene-Oligocene climate transition. Nature 461, 1110–1113. https://doi.org/10.1038/nature08447.

Peters, S.E., Carlson, A.E., Kelly, D.C., Gingerich, P.D., 2010. Large-scale glaciation and deglaciation of Antarctica during the Late Eocene. Geology 38, 723–726. https://doi.org/10.1130/G31068.1.

Pollard, D., DeConto, R.M., 2005. Hysteresis in Cenozoic Antarctic ice-sheet variations. Glob. Planet. Change 45, 9–21. https://doi.org/10.1016/j.gloplacha.2004.09.011.

Pope, V.D., Gallani, M.L., Rowntree, P.R., Stratton, R.A., 2000. The impact of new physical parametrizations in the Hadley Centre climate model: HadAM3. Clim. Dyn. 16, 123–146. https://doi.org/10.1007/s003820050009.

Rae, W.B., Zhang, Y.G., Liu, X., Foster, G.L., Stoll, H.M., Whiteford, R.D.M., 2021. Atmospheric CO_2 over the past 66 million years from Marine archives. Annu. Rev. Earth Planet. Sci. 49, 609–641. https://doi.org/10.1146/annurev-earth-082420-063026.

Scher, H.D., Martin, E.E., 2006. Timing and climatic consequences of the opening of Drake Passage. Science 312, 428–430. https://doi.org/10.1126/science.1120044.

Scher, H.D., Bohaty, S.M., Smith, B.W., Munn, G.H., 2014. Isotopic interrogation of a suspected late Eocene glaciation. Paleoceanography 29, 628–644. https://doi.org/10.1002/2014PA002648.

Śliwińska, K.K., Thomsen, E., Schouten, S., Schoon, P.L., Heilmann-Clausen, C., 2019. Climate- and gateway-driven cooling of Late Eocene to earliest Oligocene sea surface temperatures in the North Sea Basin. Sci. Rep. 9, 4458. https://doi.org/10.1038/s41598-019-41013-7.

Steinthorsdottir, M., Porter, A.S., Holohan, A., Kunzmann, L., Collinson, M., McElwain, J.C., 2016. Fossil plant stomata indicate decreasing atmospheric CO_2 prior to the Eocene–Oligocene boundary. Clim. Past 12, 439–454. https://doi.org/10.5194/cp-12-439-2016.

Tibbett, E.J., Scher, H.D., Warny, S., Tierney, J.E., Passchier, S., Feakins, S.J., 2021. Late Eocene record of hydrology and temperature from Prydz bay, East Antarctica. Paleoceanogr. Paleoclimatol. 36, e2020PA004204. https://doi.org/10.1029/2020PA004204.

Tremblin, M., Hermoso, M., Minoletti, F., 2016. Equatorial heat accumulation as a long-term trigger of permanent Antarctic ice sheets during the Cenozoic. Proc. Natl. Acad. Sci. USA 113, 11782–11787. https://doi.org/10.1073/pnas.1608100113.

Van Breedam, J., Goelzer, H., Huybrechts, P., 2020. Semi-equilibrated global sea-level change projections for the next 10 000 years. Earth Syst. Dyn. 11, 953–976. https://doi.org/10.5194/esd-11-953-2020.

Van Breedam, J., Huybrechts, P., Crucifix, M., 2021a. A Gaussian process emulator for simulating ice sheet–climate interactions on a multi-million-year timescale: CLISEMv1.0. Geosci. Model Dev. 14, 6373–6401. https://doi.org/10.5194/gmd-14-6373-2021.

Van Breedam, J., Huybrechts, P., Crucifix, M., 2021b. CLimate Ice Sheet EMulator v1.0 (CLISEMv1.0). Zenodo. https://doi.org/10.5281/zenodo.5245156.

van Hinsbergen, D.J.J., de Groot, L.V., van Schaik, S.J., Spakman, W., Bijl, P.K., Sluijs, A., Langereis, C.G., Brinkhuis, H., 2015. A paleolatitude calculator for paleoclimate studies. PLoS ONE 10, e0126946. https://doi.org/10.1371/journal.pone.0126946.

Vonhof, H.B., Smit, J., Brinkhuis, H., Montanari, A., Nederbragt, A.J., 2000. Global cooling accelerated by early late Eocene impacts? Geology 28, 687–690. https://doi.org/10.1130/0091-7613(2000)28<687:GCABEL>2.0.CO;2.

Williams, K.D., Senior, C.A., Mitchell, J.F.B., 2001. Transient climate change in the Hadley centre models: the role of physical processes. J. Climate, 2659–2674. https://doi.org/10.1175/1520-0442(2001)014<2659:TCCITH>2.0.CO;2.

Wilson, D.S., Jamieson, S.R., Barrett, P.J., Leitchenkov, G., Gohl, K., Larter, D., 2012. Antarctic topography at the Eocene-Oligocene boundary. Palaeogeogr. Palaeoclimatol. Palaeoecol. 335–336, 24–34. https://doi.org/10.1016/j.palaeo.2011.05.028.

Wilson, D.S., Pollard, D., DeConto, R.M., Jamieson, S.S.R., Luyendyk, B.P., 2013. Initiation of the West Antarctic Ice Sheet and estimates of total Antarctic ice volume in the earliest Oligocene. Geophys. Res. Lett. 40, 1–5. https://doi.org/10.1002/grl.50797.

Wright, N.M., Seton, M., Williams, S.E., Whittaker, J.M., Müller, D., 2020. Sea-level fluctuations driven by changes in global ocean basin volume following supercontinent break-up. Earth-Sci. Rev. 208, 103293. https://doi.org/10.1016/j.earscirev.2020.103293.

Zhang, Y.G., Pagani, M., Liu, Z., Bohaty, S.M., DeConto, R., 2013. A 40-million-year history of atmospheric CO_2. Philos. Trans. - Royal Soc. A, Math. Phys. Eng. Sci. 371, 20130096. https://doi.org/10.1098/rsta.2013.0096.